Journal of Directed Energy, **2**, Fall 2007, 363–375

Expected Worldwide, Low-Altitude Laser Performance in the Presence of Common Atmospheric Obscurants

S. T. Fiorino,* R. J. Bartell, M. J. Krizo, and S. J. Cusumano

Center for Directed Energy, Air Force Institute of Technology, 2950 Hobson Way, Wright–Patterson Air Force Base, Ohio 45433-7765

The directed energy modeling and simulation community can make important direct contributions to the joint warfighting community by establishing clear and fully integrated future program requirements. These requirements are best determined via analysis of the expected variability/uncertainty in system performance arising from spatial, spectral, and temporal variations in operating conditions. In the current study the expected performance of laser systems with operationally relevant output powers is assessed at 11 wavelengths between 0.40 and 10.6 μm for a number of widely dispersed locations worldwide. Scenarios evaluated include both up- and down-looking generally oblique engagement geometries over ranges up to 9,000 m in which anticipated clear air aerosols and thin layers of fog, very light rain, and light rain occur. The analysis is conducted for desert and midlatitude conditions and considers seasonal variations (summer and winter) and time-of-day variations for a range of relative humidity percentile conditions. Required dwell time corresponding to select values of probability of desired effect (P_k) is the primary performance metric used in the study. Results indicate that aerosols are the dominant laser propagation attenuators in the atmospheric boundary layer in the absence of clouds and precipitation. Furthermore, the study shows that it is important to realistically model the boundary layer to properly capture the low-altitude aerosol effects on laser propagation traversing that layer.

KEYWORDS: Aerosols, Boundary layer, Climatology, HELEEOS

1. Introduction

The directed energy modeling and simulation community can make important direct contributions to the joint warfighting community by establishing clear and fully integrated future program requirements. These requirements are best determined via analysis of the expected variability/uncertainty in system performance arising from spatial, spectral, and temporal variations in operating conditions.

In the current study the expected performance of laser systems operating at powers high enough to cause thermal blooming is assessed at 11 wavelengths between 0.40 and 10.6 μm for a number of widely dispersed locations worldwide. Scenarios evaluated include both up- and down-looking generally oblique engagement geometries over ranges up to

Received May 14, 2007; revision received September 14, 2007.
*Corresponding author; e-mail: steven.fiorino@afit.edu.

9,000 m in which anticipated clear air aerosols and thin layers of fog, very light rain, and light rain occur. The analysis is conducted for desert and midlatitude conditions and considers seasonal variations (summer and winter) and time-of-day variations for a range of relative humidity (RH) percentile conditions. Required dwell time corresponding to select values of probability of desired effect (P_k) is the primary performance metric used in the study.

2. Description of the HELEEOS Model

The Air Force Institute of Technology Center for Directed Energy developed the High Energy Laser End-to-End Operational Simulation (HELEEOS) model in part to quantify the performance variance created by the natural environment in possible high-energy-laser engagements. As such, HELEEOS includes a fast-calculating, first principles atmospheric propagation and characterization package. This package enables the creation of profiles of temperature, pressure, water vapor content, optical turbulence, and atmospheric particulates and hydrometeors as they relate to line-by-line layer extinction coefficient magnitude at wavelengths from the ultraviolet to radio frequencies. HELEEOS supports dynamic engagements in which the platform, target, and up to two optical relays can move vertically and horizontally on any heading in a true three-dimensional engagement. Engagement geometry is defined in HELEEOS by user specification of slant ranges, altitudes, headings, horizontal and vertical velocities, and horizontal and vertical accelerations. HELEEOS was developed under the sponsorship of the High Energy Laser Joint Technology Office, and its basic features have been previously described.[1]

The HELEEOS model enables the evaluation of variability in high-energy-laser propagation by incorporating probabilistic climatological data on the parameters that drive most major atmospheric effects. Atmospheric parameters investigated, such as temperature, pressure, water vapor content, optical turbulence, and atmospheric particulates, are put into vertical profiles of data for highly specific modeling scenarios. Worldwide seasonal, diurnal, and geographical spatial–temporal variation in these parameters is organized into probability density function (PDF) databases using a variety of recently available resources to include the Extreme and Percentile Environmental Reference Tables (ExPERT[14]), the Master Database for Optical Turbulence Research in Support of Airborne Laser,[2] the Global Aerosol Data Set,[8] and Air Force Weather Agency numerical weather forecasting data. GADS provides aerosol constituent number densities on a $5^\circ \times 5^\circ$ grid worldwide. ExPERT mapping software allows the HELEEOS operator to choose from specific site or regional upper-air data to characterize correlated molecular absorption, aerosol absorption, and scattering by percentile. The PDF nature of the HELEEOS atmospheric effects package enables realistic probabilistic outcome analyses.[3] Molecular scattering is computed based on Rayleigh theory. Molecular absorption effects are computed for the top 13 absorbing species using line strength information from the HITRAN 2004 database[12] in conjunction with a community standard molecular absorption continuum code. Aerosol and hydrometeor scattering and absorption are computed with the Wiscombe[15] Mie module.

Vertical profiles of molecular absorption and molecular scattering can be defined in a number of ways in HELEEOS. Thirteen standard atmospheres representing summer and winter conditions for the major climate regions are available. In addition, a large number of specific worldwide surface locations defined in ExPERT, as well as any ocean location on a $1^\circ \times 1^\circ$ latitude/longitude grid, can be selected.

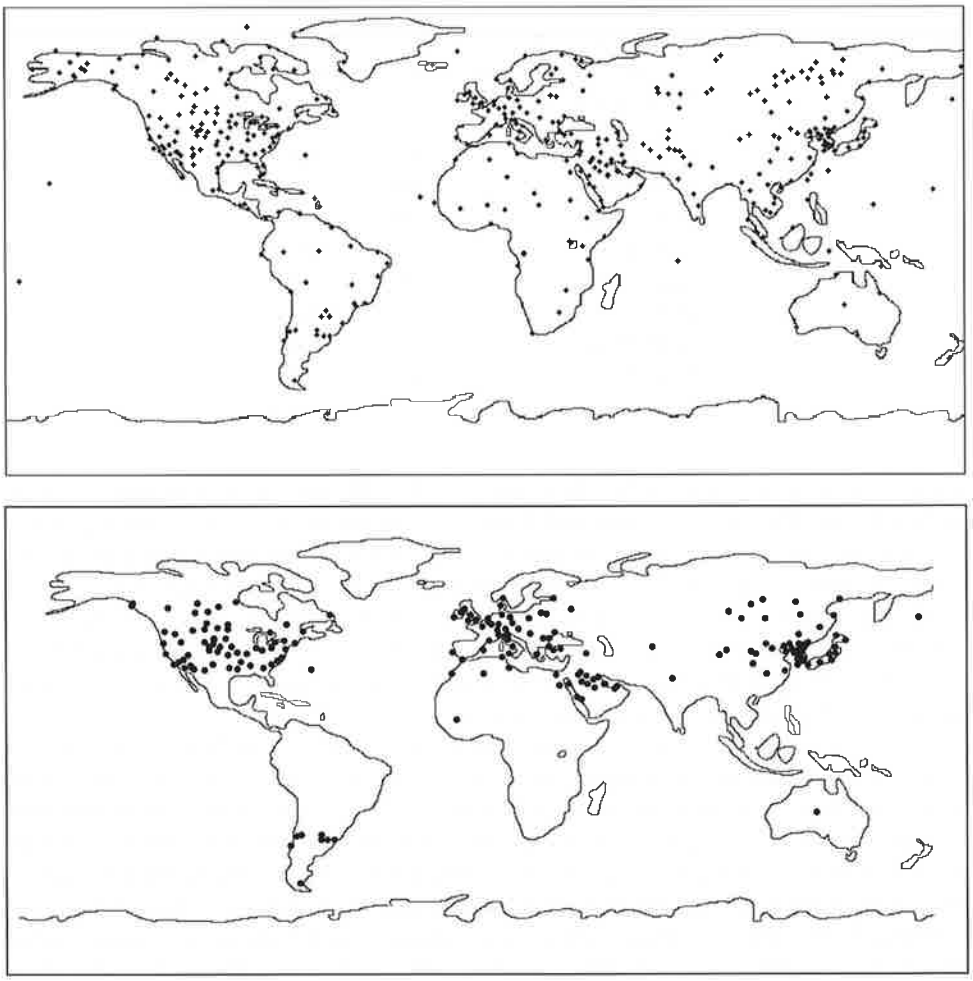

Fig. 1. The 408 ExPERT locations represented in HELEEOS (top) and the 193 midlatitude and desert sites used in this study (bottom).

Selection of an ExPERT atmosphere brings up the world map shown in Fig. 1. The black dots indicate the 408 ground sites available from ExPERT in HELEEOS. The user can also select from one of nine RH percentile conditions (ranging from 1st to 99th percentiles) to model, with the default being 50th-percentile conditions, as well as time of day in 3-h local time blocks for any of these sites.

A diverse array of aerosol vertical profiles is also available. There are 10 profiles defined using the Optical Properties of Aerosols and Clouds (OPAC) code,[6] 3 MODTRAN aerosol profiles,[13] and the windspeed-driven aerosol mixtures from the Advanced Navy Aerosol Model.[5] The aerosol profile for each ExPERT site is defined using the GADS constituent data.

HELEEOS allows the definition of five liquid water cloud types, three ice (cirrus) cloud types, water fog, ice fog, five rain rates, and a drizzle characterization in vertical layers of user-specified beginning altitude and thickness. The liquid water and ice clouds and

Table 1. Overland BL height (in meters) as a function of season and time of day

Time of day (local)	Summer	Winter
0000–0259	500	500
0300–0559	500	500
0600–0859	1,000	500
0900–1159	1,524	1,000
1200–1459	1,524	1,524
1500–1759	1,524	1,524
1800–2059	1,524	1,000
2100–2359	1,000	500

fog are characterized using OPAC distributions, while the rain cases (with the exception of drizzle) are defined using a Marshall–Palmer[10] distribution. Each atmospheric particulate/hydrometeor distribution is evaluated based on its wavelength-dependent forward and off-axis scattering characteristics and absorption effects on laser energy delivered.

Several optical turbulence profiles are available in the model; however, for this study only Hufnagel–Valley 5/7[7] is used. HELEEOS supports any user-defined wavelength from 0.40 μm to 8.6 m, with 24 specific wavelengths typically associated with laser operation available via lookup table for minimum runtime.

An important and novel aspect of the HELEEOS modeling capability is the manner in which it incorporates atmospheric boundary-layer (BL) effects into the engagement scenarios. Surface meteorological data are available in HELEEOS for the land locations for 24-h average, as well as eight 3-h local time blocks throughout the diurnal cycle. If a 3-h time block is selected, the height of the top of the atmospheric BL is dynamically adjusted, as indicated in Table 1. The BL height is set at 500 m at all times and seasons over oceanic sites.

Within the BL, the atmospheric conditions are characterized by the surface conditions for the selected site. This is accomplished according to the "well-mixed" BL qualities described in Ref. 3 and by many others. Within the well-mixed BL the water vapor mixing ratio, the aerosol number concentration, and the potential temperature are very nearly constant with altitude. While potential temperature (the temperature a parcel of air would have if it is brought dry adiabatically to a pressure level of 1,000 hPa) remains constant in the BL, temperature does vary. Temperature throughout the BL can be defined by the surface temperature and is allowed to decrease at the dry adiabatic lapse rate [Eq. (1)]. Dewpoint temperature (the temperature at which condensation occurs in a parcel of air when cooled at constant pressure) also varies throughout the BL, even though the water vapor mixing ratio remains constant. The dewpoint temperature lapses with height according to Eq. (2):

$$\left(\frac{\mathrm{d}T}{\mathrm{d}z}\right)_{\mathrm{dry}} = -\frac{g}{c_p} = -9.8\ \mathrm{K}\cdot\mathrm{km}^{-1}, \tag{1}$$

$$\left(\frac{\mathrm{d}T_d}{\mathrm{d}z}\right) = -\frac{g}{\varepsilon l_v}\frac{T_d^2}{T} \approx -1.8\ \mathrm{K}\cdot\mathrm{km}^{-1}. \tag{2}$$

In these equations, T is temperature, T_d is dewpoint temperature, z is height, g is the gravitational constant, c_p is the specific heat of air at constant pressure, ε is the ratio of the

molecular weight of water over the molecular weight of dry air, and l_v is the latent heat (enthalpy) of vaporization of water. Note that the temperature lapses at a far greater rate than the dewpoint; thus in many cases, saturation can occur within the height of the BL specified by the user. In this case the lapse rate of temperature is no longer linear with height and decreases at a rate less than the dry adiabatic rate according to Eq. (3):

$$\left(\frac{\mathrm{d}T}{\mathrm{d}z}\right)_{\text{moist}} = -\frac{g}{c_p}\frac{(1+l_v w_s)/RT}{\left(1+l_v^2 w_s\right)/c_p R_v T^2}. \tag{3}$$

The variables in Eq. (3) are the same as in Eqs. (1) and (2), and w_s is the saturation mixing ratio of water and R_v is the moist air gas constant. HELEEOS allows the above BL lapse rates to occur based on surface values for all ExPERT sites. Above the BL, HELEEOS defaults back to the upper-air regional data based on the location of the site. An important consequence of these lapse rates is that the RH varies dramatically within the BL, usually increasing from the surface to 100% or nearly so. This has a very strong effect on the aerosol size distribution—due to the RH-driven water uptake by water-soluble aerosols—that in turn strongly affects simulated laser propagation through the BL. This effect is not captured when modeling with standard atmospheric data as BL lapse rates are only allowed to occur in HELEEOS with ExPERT sites. This effect is illustrated in Fig. 2 and is most evident in the bottom plot for the midlatitude site. Midlatitude sites typically have aerosol mixtures that are predominately water soluble, while desert aerosols are typically more mineral based and are much less water soluble. Thus the top (desert) plot of Fig. 2 shows little increase in extinction with height within the BL due to increasing aerosol sizes while the bottom (midlatitude) plot exhibits a marked aerosol-induced spike in extinction with height.

In HELEEOS, as in most performance models, the laser spot at the target is modeled as a symmetric Gaussian of the form

$$\mathrm{Irr}(x, y) = \frac{K_{\text{obsc}} \cdot P}{2 \cdot \pi \cdot (\sigma_{\text{tot}} \cdot R)^2} \cdot \exp\{-0.5 \cdot [\sqrt{x^2 + y^2}/(\sigma_{\text{tot}} \cdot R)]^2\} \cdot \tau_{\text{atm}} \cdot \cos(\beta), \tag{4}$$

where $K_{\text{obsc}} = 1 - \text{obscuration}^2$, with obscuration representing the relative obscuration of the secondary mirror in the beam director telescope, and total beam spread σ_{tot} is calculated as

$$\sigma_{\text{tot}}^2 = \sigma_d^2 + \sigma_j^2 + \sigma_t^2 + \sigma_b^2 + \sigma_w^2 + \sigma_u^2, \tag{5}$$

in which $\sigma_d = k_{\text{diam}} \cdot \gamma / D \cdot BQ$ is the beam spread angle due to diffraction and BQ is the user-specified "times diffraction limited" beam quality. In HELEEOS beam quality is used to represent the effect of errors in the wavefront arising from the laser device itself, $k_{\text{diam}} = 0.4502$, a fitting parameter stemming from use of the more convenient Gaussian to represent the expected Bessel function shaped spot, $\sigma_j =$ beam spread angle due to mechanical jitter, $\sigma_t =$ beam spread angle due to optical turbulence, $\sigma_b =$ beam spread angle due to thermal blooming effects, calculated based on the combination of thermal blooming distortion number and optical turbulence strength and anchored to wave-optics predictions, $\sigma_w =$ beam spread angle due to wavefront error, $\sigma_u =$ beam spread angle due to user-specified defocus, $P =$ total output power, $R =$ slant range to the target, $\tau_{\text{atm}} =$ atmospheric transmittance, and $\beta =$ angle of incidence between the beam and the target surface normal.

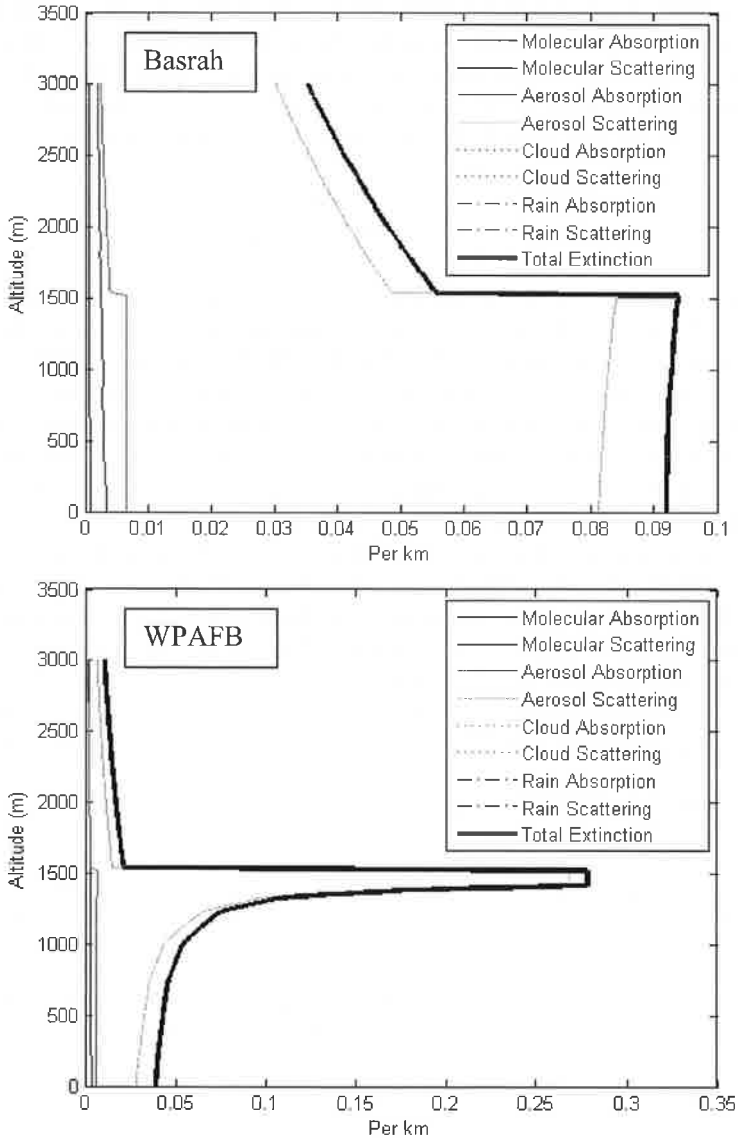

Fig. 2. Representative plots of absorption, scattering, and total extinction values for a desert site (Basrah, Iraq; top plot) and a midlatitude site (Wright–Patterson Air Force Base, Ohio; bottom plot). Plots display summer 1500–1800 local time fair weather (aerosols only) climatological extinction conditions by altitude, surface to 3,000 m. In the scenarios depicted, the total extinction is primarily due to aerosol scattering. Laser wavelength is 1.0642 μm.

3. Methodology

HELEEOS is used to examine the worldwide variance in low-altitude laser weapon system performance across a broad range of atmospheric conditions, to include effects of rain, fog, and clouds, in addition to clear air (fair weather) aerosols for an operationally relevant output

power. The metric used is required dwell time for, in this case, a 90% probability of effect. Required dwell time is one of several operationally oriented metrics available in HELEEOS. Results are presented as histograms, based on wavelength, probability of occurrence, and required dwell time (Figs. 3 and 4). Another goal of this study is to geographically map the most effective wavelength, from a limited set of wavelengths, for several atmospheric conditions.

Parameters used throughout the study include the following:

- Aperture 0.5 m, uniform beam with 0.1 relative central obscuration
- Turbulence conditions Hufnagel–Valley 5/7
- Tilt-only correction; no adaptive optics
- Assumed lethal fluence 5 kJ cm^{-2}
- No jitter

Parameters varied as part of the study include the following:

- 11 wavelengths: 0.40, 0.56, 0.68, 1.00, 1.054, 1.0642, 1.31525, 1.586, 1.624, 3.80, and 10.60 μm
- 193 desert and midlatitude ExPERT locations worldwide
- Atmospheric conditions:
  - 5th-, 50th-, 95th-percentile RH
  - 4 times of day (3-h local time blocks)
  - Summer and winter
  - Clear sky aerosols
  - Very light rain (2 mm h^{-1}), 1,525 m to the surface
  - Light rain (5 mm h^{-1}), 1,525 m to the surface
  - Fog, 150 m thick
- 4 Geometries:
  - Air-to-surface, 2,000-m slant range
  - Air-to-surface, 4,000-m slant range
  - Air-to-surface, 9,000-m slant range
    - Platform altitude 1,525 m
    - Target altitude 0 m
    - Platform velocity 100 m s^{-1} toward stationary target
  - Surface-to-air, 4,000-m slant range
    - Platform altitude 0 m
    - Target altitude 1,525 m
    - High speed (1,060 m s^{-1}) diagonally crossing target

For all air-to-surface geometries the platform is at 1,525-m altitude; for all surface-to-air geometries, the platform is at the surface with the target at an altitude of 1,525 m. The study is thus restricted to oblique paths through the daytime atmospheric BL depth.

4. Results

This section includes a limited selection of results from the current study. Figure 3 compares expected summer performance for midlatitude and desert conditions across the 11 wavelengths for the 4,000-m slant range air-to-surface scenario, for all times of day and all RH percentile conditions considered. Higher probabilities in a particular required dwell time bin for a specific wavelength mean that more of the scenarios modeled indicated that

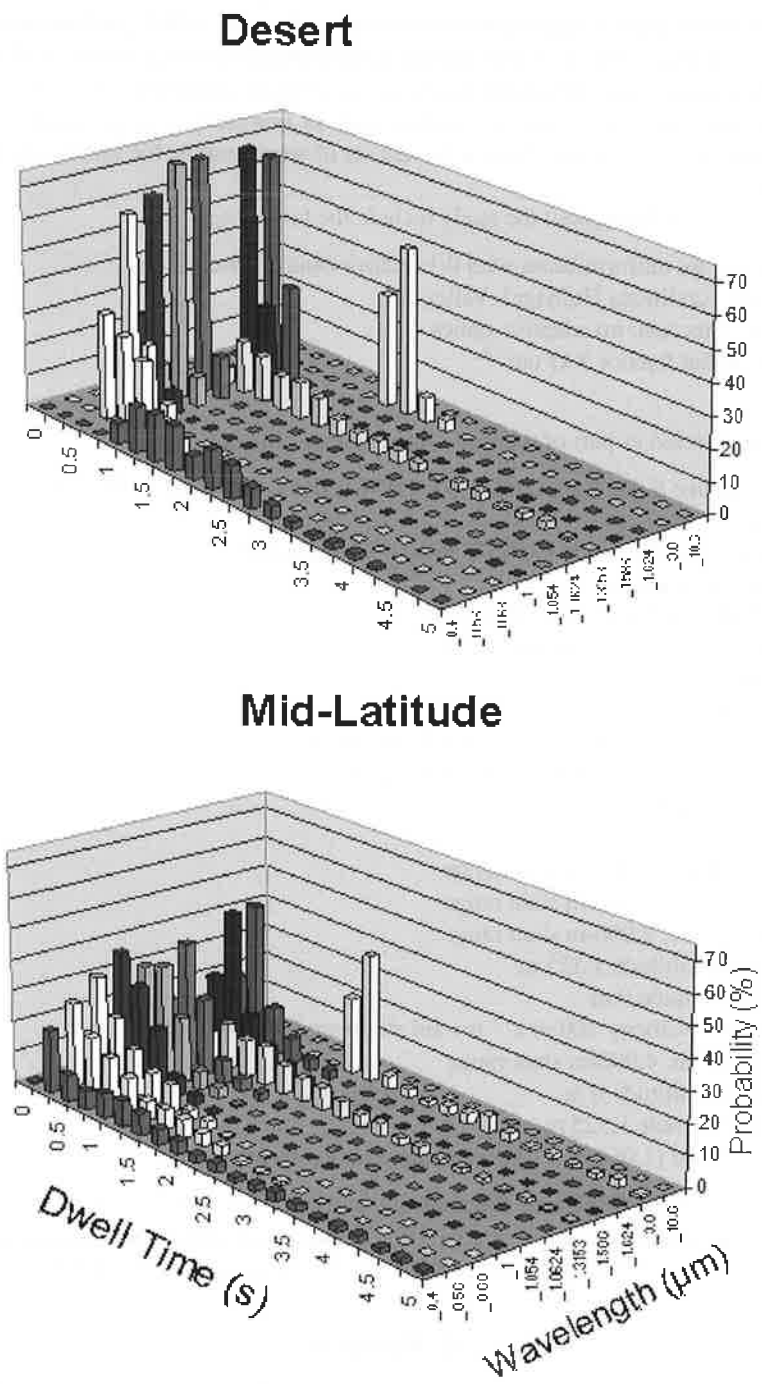

Fig. 3. Comparison of desert and midlatitude performance in summer conditions. Incorporates all times of day, all RH percentiles, HELEEOS scaling laws; air-to-surface geometry, 4,000-m slant range, and fair weather aerosols. Platform altitude 1,525 m.

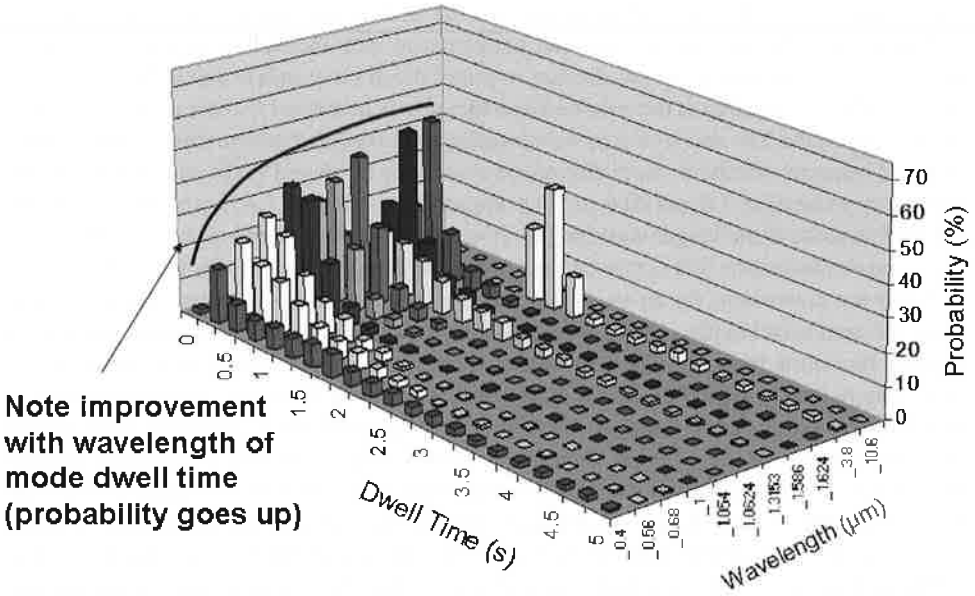

Fig. 4. Worldwide (193 desert and midlatitude sites) result for the 4,000-m slant range, air-to-ground scenario, for all locations, both seasons, all times of day, all RH percentiles, and fair weather aerosols only. Platform altitude 1,525 m.

particular result. For each wavelength, probability sums to 100% across all possible dwell time bins. In Fig. 3, the highest probabilities in both the desert and midlatitude regions are clustered toward required dwell times of less than 1 s for all wavelengths except 3.8 and 10.6 μm. Performance is generally better in light-wind desert conditions because midlatitude aerosols are more water soluble and therefore more affected by the higher and height-varying RH conditions, as shown in Fig. 2. Under midlatitude conditions, performance is similar across all the wavelengths evaluated with two exceptions: 0.4 μm, which is affected by Rayleigh scattering (also true in desert conditions), and 1.31525 μm, which is affected significantly by water vapor absorption. Performance at 3.8 and 10.6 μm is impacted by the diffraction limitations of the fixed 0.5-m aperture diameter used in this study.

Of critical importance in the results of Fig. 3 is the angle in which the slant path traverses the atmospheric BL. In the case shown in Fig. 3, where the oblique 4,000-m slant path starts at 1,525 m and goes to the surface, the laser beam must propagate a significant distance in the midlatitude spike of extinction due to water-soluble aerosols. If the slant path is more vertical, the effects of the midlatitude spike are reduced. This potentially has an interesting effect on the desert/midlatitude comparison, as a more vertical slant path has less of an effect on the desert expected performance because the desert extinction is more constant with altitude (refer to Fig. 2). Fiorino et al.[4] conducted a similar modeling study with a higher platform altitude (3,000 m) over a more vertical slant path (6,000 m) and found the expected performance at the desert sites to be slightly worse than at the midlatitude sites.

Figure 4 is a global result for the 4,000-m slant range, air-to-surface scenario, for all locations, both seasons, all times of day, and all RH percentile conditions, clear sky aerosols only. Here we see expected performance improve as wavelength is increased from the visible to the shortwave infrared, with the exceptions again of 1.31525 μm, which is affected

significantly by water vapor absorption, and the diffraction-limited wavelengths of 3.8 and 10.6 μm. This increase in expected performance with increasing wavelength is most evident in the probabilities at the shortest required dwell times and is due to Mie scattering aerosol effects.[9] Notably, if the assumed aperture size is increased to remove the diffraction limitations on the 3.8- and 10.6-μm wavelengths, their modeled performance in the context of Fig. 4 becomes similar to the performance shown for 1.586 and 1.624 μm. While aerosol effects are reduced at 3.8 and 10.6 μm as compared to 1.586 and 1.624 μm, the reason that the performance at the longer wavelengths is not significantly better is due to the increased water vapor absorption that occurs at the longer wavelengths (especially 10.6 μm).

While not shown here, the air-to-surface 9,000-m slant range results are much more varied. Near-infrared wavelengths (in this study, wavelengths from 1 to 1.624 μm) not affected by thermal blooming have the best performance, but simulated expected dwell times are 10 times longer than in the 4,000-m case and likely would not be effective. The case of surface-to-air versus a high-speed target at 4,000-m slant range required dwell times three to four times longer than in the 4,000-m slant range air-to-surface case. The simulations suggest that there is some operational capability in very light rain (2 mm h^{-1}) conditions for slant ranges of 4,000 m and shorter for the near-infrared wavelengths not affected by thermal blooming. All wavelengths become ineffective in light rain (5 mm h^{-1}) conditions, even at 4,000-m slant range. The modeled results also show that there is air-to-surface operational capability with a 150-m-thick fog layer present for near-vertical slant ranges, on the order of 2,000 m from 1,500-m altitude.

The second phase of the study involves geographically mapping (or geomapping) the most effective wavelength for several atmospheric conditions. In this part of the study a subset of five wavelengths is considered: 0.68, 1.0642, 1.31525, 1.586, and 3.80 μm. Four atmospheric conditions are evaluated:

- Clear sky aerosols only
- Very light rain (2 mm h^{-1}) plus aerosols
- Light rain (5 mm h^{-1}) plus aerosols
- Fog (150-m-thick deck) plus aerosols

The metric used to determine best performance is lowest median dwell time for 90% probability of effect.

Figure 5 is a mapping of the results for a nearly horizontal slant path of 9,000 m from a platform at 1,525 m for aerosols-only under winter conditions. The mapping for summer conditions is very similar. The 1.586-μm wavelength is the most commonly selected wavelength overall, as one might expect from the shorter slant path results shown in Fig. 4. A few sites in Europe and the Mediterranean show the 1.0642-μm wavelength. The selection of the 1.31525-μm wavelength in central Canada, despite the effects of water vapor absorption, is attributed to the low absolute humidity of the winter conditions and is taken as an indicator that in many cases aerosol scattering effects are of more importance in relatively short, lower atmospheric engagements than thermal blooming effects.

Figure 6 displays the results for the same engagement geometry as Fig. 5 but for very light rain conditions in summer. In this case, the visible 0.68-μm wavelength dominates as there is virtually no absorption by liquid water drops/droplets at visible wavelengths.[11] Despite the extreme nature of this scenario with a nearly horizontal 9-km slant path through 2 mm h^{-1} rainfall, the 1.0642-μm wavelength was selected at two North American sites and one Asian site. This suggests that near-infrared laser designators may maintain some operational capability in light rain environments.

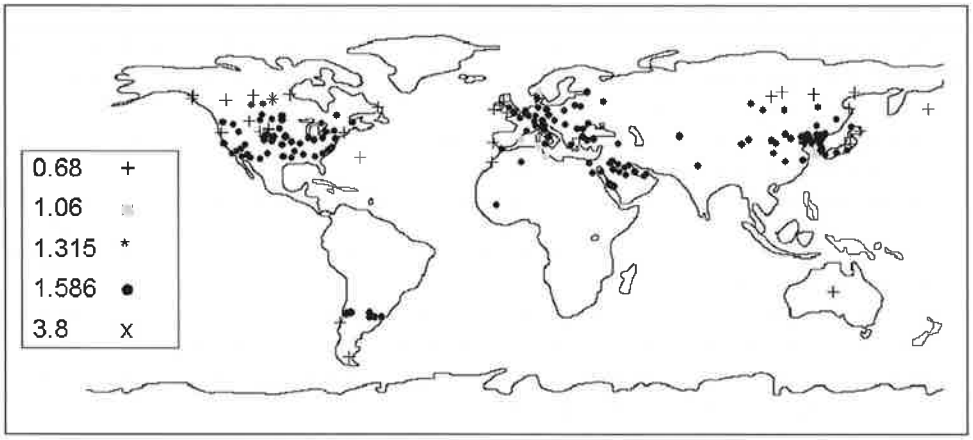

Fig. 5. Geomapping of the aerosols-only results for winter conditions. Incorporates all times of day, all RH percentiles, HELEEOS scaling laws; air-to-surface geometry, 9,000-m slant range air-to-ground. Platform altitude 1,525 m.

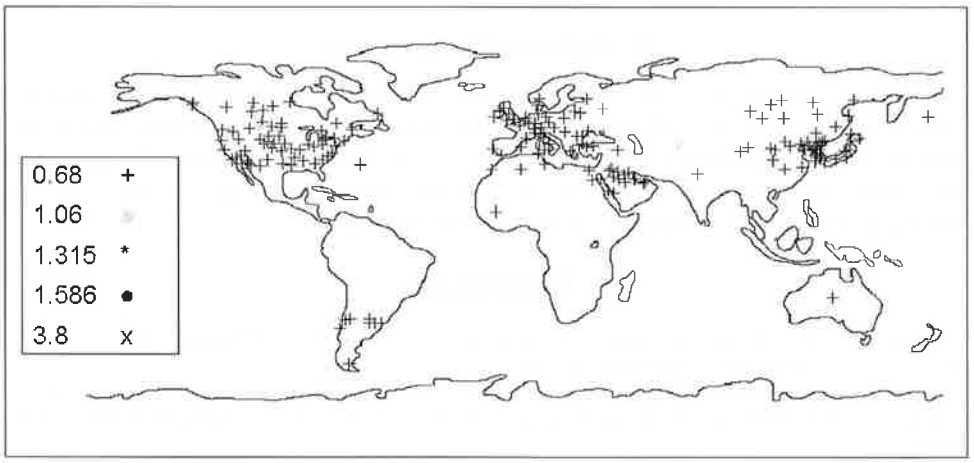

Fig. 6. Geomapping of the very light rain (2 mm h^{-1}) results for summer conditions. Incorporates all times of day, all RH percentiles, HELEEOS scaling laws; air-to-surface geometry, 9,000-m slant range air-to-ground. Platform altitude 1,525 m.

5. Summary/Conclusions

In this study the expected performance of laser systems operating at powers high enough to cause thermal blooming is assessed at 11 wavelengths between 0.40 and 10.6 μm for a number of widely dispersed locations worldwide. Midlatitude and desert scenarios are evaluated to include both up- and down-looking generally oblique engagement geometries over ranges up to 9,000 m in which fair weather aerosols and thin layers of fog, very light rain, and light rain are modeled. The analysis considers summer and winter seasonal variations and time-of-day variations for a range of RH percentile conditions. The HELEEOS performance model is used to model the scenarios.

In addition to the study results summarized below, a leading conclusion of the research is the importance of accurately characterizing the physical structure of the atmospheric BL when simulating laser propagation through the lowest levels of the atmosphere. Use of a typical standard atmospheric reference will not properly capture the BL decrease of temperature and increase of RH with height, and therefore will not inject realistic aerosol extinction effects into the simulated scenarios.

Overall observations from this modeling study include the following:

- Expected performance of laser systems at low altitudes is very sensitive to slant path angle through the atmospheric BL.
- Operational high-energy-laser capability exists to some extent in the presence of very light rain or fog layers near the ground over a limited range of geometries.
- 1.0642-μm laser designators likely have operational capability in very light rain even over very long nearly horizontal slant paths.
- Wavelengths around 0.68 μm perform best in the presence of liquid precipitation.
- Aerosol effects dominate in clear sky, low-altitude engagements.
- Longer wavelengths are less attenuated by aerosols; however, water vapor absorption and diffraction effects in the mid- and longwave infrared counteract the reduced aerosol attenuation to allow peak performance at $\sim$1.6 μm.

6. Acknowledgments

The authors recognize the outstanding support of the High Energy Laser Joint Technology Office, Albuquerque, New Mexico, and two reviewers whose comments, suggestions, and critical insights significantly improved the paper. The views expressed in this paper are those of the authors and do not necessarily reflect the official policy or position of the Air Force, the Department of Defense, or the U.S. Government.

References

[1]Bartell, R.J., G.P. Perram, S.T. Fiorino, S.N. Long, M.J. Houle, C.A. Rice, Z.P. Manning, M.J. Krizo, D.W. Bunch, and L.E. Gravley, Proc. SPIE **5792**, 76 (2005).

[2]Bussey, A.J., J.R. Roadcap, R.R. Beland, and G.Y. Jumper, "Master Data Base for Optical Turbulence Research in Support of Airborne Laser," Air Force Research Laboratory Technical Report, AFRL-VS-TR-2000-1545, 2000.

[3]Fiorino, S.T., R.J. Bartell, G.P. Perram, D.W. Bunch, L.E. Gravley, C.A. Rice, Z.P. Manning, and M.J. Krizo, J. Directed Energy **1**(4), 347 (2006).

[4]Fiorino, S.T., R.J. Bartell, G.P. Perram, M.J. Krizo, D.J. Fedyk, B.W. Wisdom, and S.J. Cusumano, Proc. SPIE **655104** (2007).

[5]Gathman, S.G., A.M.J. van Eijk, and L.H. Cohen, Proc. SPIE **3433**, 41 (1998).

[6]Hess, M., P. Koepke, and I. Schult, Bull. Am. Met. Soc. **79**, 831 (1998).

[7]Hufnagel, R.E., "Propagation Through Atmospheric Turbulence," in *The Infrared Handbook*, edited by W.L. Wolfe and G.J. Zissis, Infrared Information Analysis Center, Ann Arbor, MI (1985).

[8]Koepke, P., M. Hess, I. Schult, and E.P Shettle, "Global Aerosol Data Set," Max Planck Institute Meteorologie Hamburg Report 243, 1997.

[9]Liou, K.N., *An Introduction to Atmospheric Radiation*, 2nd ed., Chapter 3, p. 96, Academic Press (2002).

[10]Marshall, J.S., and W.M. Palmer, J. Meteor. **5**, 165 (1948).

[11]Petty, G.R., *A First Course in Atmospheric Radiation*, Chapter 12, p. 367, Sundog Publishing, Madison, WI (2004).

[12]Rothman, L.S., C.P. Rinsland, A. Goldman, S.T. Massie, D.P. Edwards, J.M. Flaud, A. Perrin, C. Camy-Peyret, V. Dana, J.Y. Mandin, J. Schroeder, A. McCann, R.R. Gamanche, R.B. Wattson, K. Yoshino, K.V. Chance, K.W. Jucks, L.R. Brown, V. Nemtchinov, and P. Varanasi, "The HITRAN Molecular Spectroscopic Database and HAWKS (Hitran Atmospheric Workstation), 2004 edition," 2004.

[13]Shettle, E.P., and R.W. Fenn, "Models for the Aerosols of the Lower Atmosphere and the Effects of Humidity Variations on Their Optical Properties," Air Force Geophysics Laboratory Technical Report, AFGL-TR-79-0214, 1979.

[14]Squires, M.F., B.A. Bietler, S.T. Fiorino, D.L. Parks, F.W. Youkhana, and H.D. Smith, "A Method for Creating Regional and Worldwide Datasets of Extreme and Average Values," Institute of Environmental Sciences 1995 Proceedings, 41st Annual Meeting, 1995.

[15]Wiscombe, W.J., Appl. Opt. **19**(9), 1505 (1980).

The Authors

Mr. R. J. Bartell received his B.S. degree in physics from the U.S. Air Force Academy as a distinguished graduate in 1979. He received his M.S. degree from the Optical Sciences Center, University of Arizona, in 1987. He is currently a Research Physicist with the Center for Directed Energy at the Air Force Institute of Technology, where he leads the development of the High Energy Laser End-to-End Operational Simulation (HELEEOS) model.

Dr. Salvatore J. Cusumano is the Director of the Center for Directed Energy located at AFIT. He received his Ph.D. in control theory from the University of Illinois in 1988, a Master's in electrical engineering from AFIT in 1977, and a Bachelor's in electrical engineering from the Air Force Academy in 1971. The Center collaborates on directed energy research topics, both high-power microwaves (HPM) and high-energy lasers (HEL), throughout the DoD community. Dr. Cusumano's research interests span his 25 years of experience in directed energy and include resonator alignment and stabilization, intracavity adaptive optics, phased arrays, telescope control, pointing and tracking, adaptive optics, and component technology for directed energy. He holds two patents (jointly) for his work in phased arrays.

Lt. Col. Steven Fiorino is an Assistant Professor of atmospheric physics at the Air Force Institute of Technology (AFIT) and a research faculty member within AFIT's Center for Directed Energy. He has B.S. degrees from Ohio State (1987) and Florida State (1989) universities, an M.S. in atmospheric dynamics from Ohio State (1993), and a Ph.D. in physical meteorology from Florida State (2002). His research interests include microwave remote sensing, development of weather signal processing algorithms, and atmospheric effects on military systems such as high-energy lasers and weapons of mass destruction.

Mr. Matthew Krizo is currently the lead programmer for the HELEEOS project as part of AFIT's Center for Directed Energy. He has been working with HELEEOS since 2004. He oversees the development of the model and the incorporation of new capabilities into HELEEOS. He received a B.S.E.E in 2005 from Cedarville University. He is currently working on an M.S.E.E from the University of Dayton and is expected to graduate in spring of 2008.